J. Fluid Mech. (1977), *vol.* 82, *part* 1, *pp.* 147–159
Printed in Great Britain

Upstream influence and Long's model in stratified flows

By P. G. BAINES
C.S.I.R.O. Division of Atmospheric Physics, Aspendale, Victoria, Australia

(Received 12 May 1976 and in revised form 10 December 1976)

This paper describes an experimental study of a stratified fluid which is flowing over a smooth two-dimensional obstacle which induces no flow separation and in which effects of viscosity and diffusion are not important. The results are restricted to fluid of finite depth. Various properties of the flow field, in particular the criterion for the onset of gravitational instability in the lee-wave field, are measured and compared with the theoretical predictions of Long's model. The agreement is found to be generally poor, and the consequent inapplicability of Long's model is explained by the failure of Long's hypothesis of no upstream influence, which is demonstrably invalid when stationary lee waves are possible. The obstacle generates upstream motions with fluid velocities which appear to be of first order in the obstacle height. These motions have some of the character of shear fronts or columnar disturbance modes and have the same vertical structure as the corresponding lee-wave modes generated downstream. They result in a reduced fluid velocity upstream below the level of the top of the obstacle, together with a jet of increased fluid velocity above this level which pours down the lee side of the obstacle. This phenomenon becomes more pronounced as the number of modes is increased.

1. Introduction

The nature of stratified flow over obstacles and the question of what influence (if any) the presence of an obstacle exerts far upstream have been controversial issues for many years (see, for example, Benjamin 1970; Turner 1973, chap. 3). Long's (1955) theoretical model, which applies to two-dimensional incompressible inviscid flow, has provided a tantalizingly simple procedure for calculating the complete flow field without approximations. However, it requires the assumptions (*a*) that the flow is steady and (*b*) that the horizontal kinetic energy $\frac{1}{2}\rho(z)\,U(z)^2$ (ρ is the fluid density and U the horizontal fluid velocity) is independent of the height z far upstream. For the application of the model to initially uniform flow (i.e. ρU^2 independent of z) which is modified by the introduction of an obstacle, assumption (*b*) contains implicitly the assumption of no (or at least negligible) influence of the obstacle on the fluid far upstream, commonly termed 'Long's hypothesis'. The complete equations for the flow field may then be expressed in a form in which the nonlinear advection terms vanish identically, and the equations reduce to a classical Helmholtz equation for which methods of solution may be found. This raises another long-standing question, namely whether the flow field so obtained is 'special' and lacks some properties which would be present with other, more general, upstream velocity profiles.

Long's model has been applied to two-dimensional flow over an obstacle in a channel

of finite depth by Long (1955), Yih (1960), Drazin & Moore (1967), Miles (1968*a*), Pao (1969), Davis (1969) and Pekelis (1972) and to flow of infinite depth by Miles (1968*a*, *b*), Miles & Huppert (1969), Huppert & Miles (1969) and Pao (1969).† Long's hypothesis has also been employed, consciously or unconsciously, in a number of numerical studies in the meteorological literature. The question of the uniqueness of solutions to the mathematical problem posed by Long's model has been discussed for the finite-depth case by Grimshaw (1968), who showed that the problem was well posed for any finite obstacle provided it satisfied a simple convexity condition (effectively excluding mushrooms).

Long's model has its intrinsic limitations. We define h to be the obstacle height, D the channel depth, N the Brunt–Väisälä frequency and $K = ND/\pi U$. Segur (1971) showed that if $[K] > [K(1-h/D)]$, where $[K]$ denotes the largest integer $\leqslant K$, then as the length of the obstacle was increased (its shape was assumed to be approximately rectangular) the lee-wave amplitudes tended towards infinitely large magnitudes and the solution became physically unrealistic. Conversely, if the above expression was an equality no such behaviour occurred. These results were established within the confines of Long's model and indicate limitations based on h/D and the obstacle length. For infinite depth, the work of Miles and Huppert cited above indicates that Long's model becomes inapplicable owing to instability in the lee-wave field when $R = Nh/U$ becomes greater than a number which depends on the obstacle shape, but is generally of order unity. Hence there are limitations to the applicability of Long's model which are independent of the upstream assumption.

The validity of Long's hypothesis has been discussed at length by McIntyre (1972), who performed an expansion with the height of the mountain as small parameter and showed that to second (and probably all) orders no effects far upstream are obtained by this procedure, apart from some weak second-order columnar motions generated by nonlinear interactions in the lee-wave tails, in the finite-depth case. This work has now become the chief justification for the use of Long's model, not only for two-dimensional flow but also for axisymmetric flow around obstacles in a rotating fluid, for which it has been used by Miles (1972) in the first of a series of papers, the latest being Miles (1975).

There is also a class of theoretical studies of stratified flow in the limit of very slow motion which predicts, among other things, upstream blocking of the fluid below the top of the obstacle, extending to infinity. This will be discussed in more detail in a later paper (Baines 1977) and for present purposes it suffices to say that the proponents of Long's model assume that the flow speed is sufficiently high for such effects to be negligible. Justification for Long's hypothesis has also been sought from the work of Trustrum (1964), who showed that a dipole with its axis horizontal (frequently used to model an obstacle, by analogy with potential flow) on a horizontal boundary produced no effects far upstream.

Corresponding experimental studies have been relatively few, there being only three or four which have a direct bearing on the validity or otherwise of Long's model. The first of these was carried out by Long using smooth flat obstacles and described in his original paper (Long 1955), where the theoretical and observed flow fields were presented for visual comparison and showed general similarity provided that K and R were not too large. If these conditions were not satisfied, blocking was observed upstream below the top of the obstacle and multiple jets above it, extending an unknown distance

† This list is probably far from complete.

upstream. Long assumed (incorrectly in view of the results of Grimshaw 1968) that the solution did not exist if the obstacle was higher than the lowest nodal line of a lee wave, and also that the solutions could be invalidated if overturning occurred in the lee waves, causing turbulence. He thus concluded that the model was a good approximation to reality if these two latter conditions were not violated. A similar comparison of lee-wave observations with the model has been made by Droughton & Chen (1971), with similar conclusions.

Davis (1969) also carried out a combined theoretical and experimental study, using taller obstacles ($\frac{3}{16}$ and $\frac{1}{4}$ of the channel depth) consisting of vertical barriers and triangles. He observed considerable turbulence downstream in the wake of the mountain, and also in rotor regions when the flow was subcritical with respect to about three or four lee-wave modes. He concluded that this was responsible for the observed discrepancy between the theoretical and experimental flows, and that consequently Long's model was useful only when a small number of lee-wave modes were present. However, the obstacle shapes chosen and particularly the presence of sharp corners tended to induce flow separation and turbulence on the lee side which would not be present for other, smoother shapes, so that these results do not provide a good test of the usefulness of Long's model in such cases. Some effects (not described) were observed upstream but were assumed to be insignificant.

After the completion of most of the work described in this paper the author became aware of the work of Wei, Kao & Pao (1975), who studied upstream effects of flow over vertical barriers and circular obstacles. Various columnar disturbance modes – horizontal velocity profiles with sinusoidal vertical structure appropriate to the subcritical lee-wave modes – were observed at considerable distances upstream (up to three times the depth) with, in some cases, little change in amplitude. The presence of these was attributed to flow separation behind the obstacle causing an expanding region of turbulent mixed fluid as the obstacle moved along, resulting in a source-like obstacle producing the upstream flow in the manner described by Wong & Kao (1970) and Trustrum (1964). This explanation would seem unlikely since a turbulent wake does not really constitute source-like behaviour (because there is no change in the fluid volume, as the wake grows at the expense of the surrounding stratified fluid).

In summary, it would appear that Long's model provides a satisfactory description of the flow field in some cases, but that the region of its validity is ill defined and the manner in which it breaks down is not at all understood. The original aim of the work described in this paper was to test theoretical criteria for instability and rotor formation obtained from Long's model, using smooth obstacles which did not induce flow separation purely because of their shape. The establishment of such criteria is one of the main questions to which Long's model has been applied (Miles 1968*a*, etc), and it is of practical significance for prediction of turbulence (clear air and otherwise) near mountains in the atmosphere and also in the oceans.

The plan of the paper is as follows: in § 2 the experimental apparatus and procedure are described; in § 3 various flow properties obtained from Long's model are compared with observations and considerable discrepancy is found, leading to a study of the flow observed upstream of the obstacle, which is described in § 5. The stagnant or 'rotor' regions found in the large amplitude lee waves are described in § 4 and the conclusions are given in § 6.

For the analogous system of motion along the axis of a rotating fluid, experiments for the axially symmetric case described by Pritchard (1969) and Maxworthy (1970) show some features corresponding to those reported here.

2. The experimental apparatus

The experiments were carried out in a rectangular Perspex-sided tank of length 3·66 m and width 0·23 m filled with salt-stratified water to a depth which was varied but was typically 0·3 m. The vertical density gradient was constant from top to bottom, and the total density difference was typically 0·4 %.† The fluid motion was generated by towing the obstacle (or 'mountain') along the bottom of the tank from right to left (as seen by the observer), starting from a position 0·56 m from the right-hand end.

In order to be able to observe the flow relative to the mountain, a pair of tracks was fitted alongside the tank to support a moving carriage which travelled on rollers and on which was mounted a camera. The carriage could be connected to the electric motor used for towing the mountain by means of steel wire, so that both mountain and carriage could travel along the tank together at any chosen speed. Flow visualization was by means of neutrally buoyant expanded-polystyrene beads, which had a range of densities covering that of the fluid.

In contrast with the experiments of Davis (1969), who used vertical barriers and triangular-shaped mountains, the present experiments used obstacles with the smooth 'Witch of Agnesi' profile, given by

$$z = ha^2/(x^2+a^2), \tag{2.1}$$

where x and z are horizontal and vertical co-ordinates respectively. Two mountain shapes were used: for the smaller, the height $h = 2{\cdot}8$ cm and the 'half-width' $a = 4{\cdot}0$ cm; for the larger, $h = 6{\cdot}26$ cm and $a = 4{\cdot}95$ cm. For these shapes no separation of the flow from the bottom boundary on the lee side of the obstacle was observed, except in one extreme case (not discussed here) where the channel depth was less than twice the mountain height.

For nearly all of the experimental runs described in this paper, viscous boundary layers on the top, bottom and side walls had a small effect on the main features of the flow. Towing times were mostly less than 200 s, which gives a single boundary-layer thickness of $(\nu t)^{\frac{1}{2}} \lesssim 1{\cdot}4$ cm. For most runs, the Reynolds number (based on the obstacle height) was somewhat greater than 300.

3. Long's model: comparison of predictions with observations

Long (1955) showed that, under assumptions (*a*) and (*b*) of §1, in a channel of depth D the equations of motion could be reduced to

$$\nabla^2\delta + K^2\delta = 0, \quad K = ND/\pi U, \tag{3.1}$$

† The tank and the method of filling it are the same as those described in McEwan & Baines (1974), but with no contraction and with the paddles vertical.

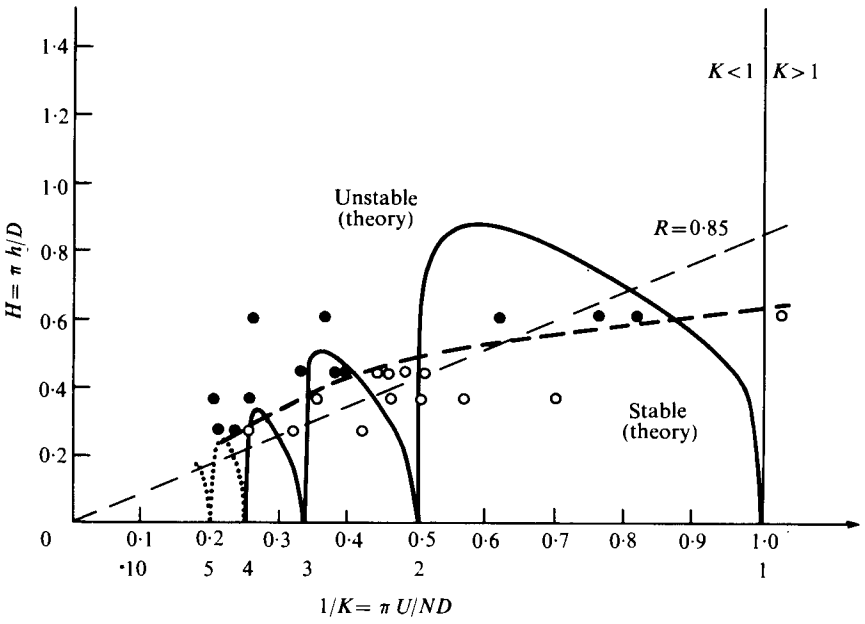

FIGURE 1. Experimentally observed conditions for gravitational instability in the lee waves for the Witch of Agnesi profile with $a/D = 0{\cdot}095$. ●, unstable points; ○, stable points; — —, simplest curve separating these points; ——, corresponding theoretical curve obtained from Long's model; — —, $R = Nh/U = 0{\cdot}85$, which is the critical value of R for the case of infinite depth (Miles & Huppert 1969).

where $\delta(x, z)$ is the vertical displacement of the streamline passing through the point (x, z) from its elevation far upstream. The boundary conditions are then

$$\left.\begin{array}{lll} \delta \to 0 & \text{as} & x \to -\infty, \\ \delta = 0 & \text{on} & z = D, \\ \delta = h(x) & \text{on} & z = h(x), \quad \text{where} \quad h(x) \to 0 \quad \text{as} \quad x \to -\infty. \end{array}\right\} \tag{3.2}$$

These constitute the equations of Long's model. Miles (1968*a*) has shown that the solution to this system may be expressed in the form

$$\delta(x,z) = \int_{S'} \left\{ \frac{\partial G}{\partial n}\, \delta(\xi,\eta) - G(\xi,\eta) \frac{\partial \delta}{\partial n} \right\} dl, \tag{3.3}$$

where S' is the surface of the obstacle, n denotes the outwardly directed normal to the surface and $G(x, z/\xi, \eta)$ is the appropriate Green's function. For values of K between the integers N and $N+1$ the appropriate expression for G is

$$\begin{aligned} G = &-\frac{2}{\pi} H(x-\xi) \sum_{n=1}^{N} \alpha_n^{-1} \sin \alpha_n (x-\xi) \sin n\eta \sin nz \\ &+ \frac{1}{\pi} \sum_{n=N+1}^{\infty} \alpha_n^{-1} \exp\left(-\alpha_n |x-\xi|\right) \sin n\eta \sin nz, \end{aligned} \tag{3.4}$$

where H is the Heaviside step function, all lengths have been made dimensionless using the length D/π and $\alpha_n = |K^2 - n^2|^{\frac{1}{2}}$.

These equations were solved to obtain various properties of the flow field using the

numerical scheme of Davis (1969), whereby $\partial\delta/\partial n$ was evaluated at a set of grid points on the lower boundary from a finite-difference form of (3.3) applied to the lower boundary, these values then being used in (3.3) to obtain δ at other points of the flow field. Fifty-one grid points were normally used but on occasions the accuracy was checked by using one hundred and even two hundred grid points. The procedure was checked for self-consistency, and with Miles' solution for flow over a semicircular object. Satisfactory agreement was obtained, and the accuracy of any given point was of the order of 0·1 % of the channel depth.

Using this procedure, for fixed values of K the obstacle height h was varied and the flow field searched to obtain the smallest height for which a streamline somewhere in the flow became vertical, i.e.

$$\partial\delta/\partial z = 1. \tag{3.5}$$

As h was increased further $\partial\delta/\partial z$ became greater than unity in the region where this occurred, indicating static instability and 'rotor' formation. The resulting curve for this criterion as a function of K for the Witch of Agnesi profile (2.1) with $a/D = 0{\cdot}095$ is given by the solid line in figure 1. Similar curves for objects of unknown shape were given in figure 2 of Long (1955), who showed that this general shape with 'humps' between integer values of K persisted for very large K. Long's model solutions become singular when K has integer values. For $1 < K < 2$, when only the first lee-wave mode is present, the point of incipient instability occurs at the upper boundary; for

$$2 < K < 3$$

it occurs at mid-depth, and as K increases it occurs at a progressively lower depth (depending on the lee-wave modes present) and, perhaps, closer to the obstacle.

To test these results, the obstacle was towed along the tank at constant speed starting from rest in the manner described in § 2, and successive time-exposure photographs were taken of the evolving velocity field from the moving carriage. As far as could be determined visually, the flow field close to the obstacle (including the potentially unstable region) appeared to reach a steady state within a towing distance of about 2 m for the cases reported here. When unstable regions occurred they were observed to result from streamlines becoming vertical (with positive gradient) and overturning, so that the theoretical criterion $\partial\delta/\partial z = 1$ is appropriate, and this instability occurred near the location predicted by Long's model. However, the conditions which were observed to be stable (open circles in figure 1) and unstable (closed circles) bear little relation to the theoretical predictions of Long's model. The experimental points representing stable and unstable conditions are separated by the heavy dashed line in figure 1. It is possible that some points which were marginally stable would eventually become unstable if the towing distance were longer, causing the dashed curve to be lowered slightly, but this would hardly improve the agreement. Also the value of a/D differed from the theoretical one of 0·095 in the range

$$0{\cdot}13 < a/D < 0{\cdot}30$$

with varying D, but this is expected to affect the theoretical curve only slightly (Long 1955). The dips in the theoretical curve were specifically looked for very closely, but no such behaviour was evident in the observations. Streak photographs of the final steady-state flow fields for some of the above experimental points are shown in figure 2 (plate 1).

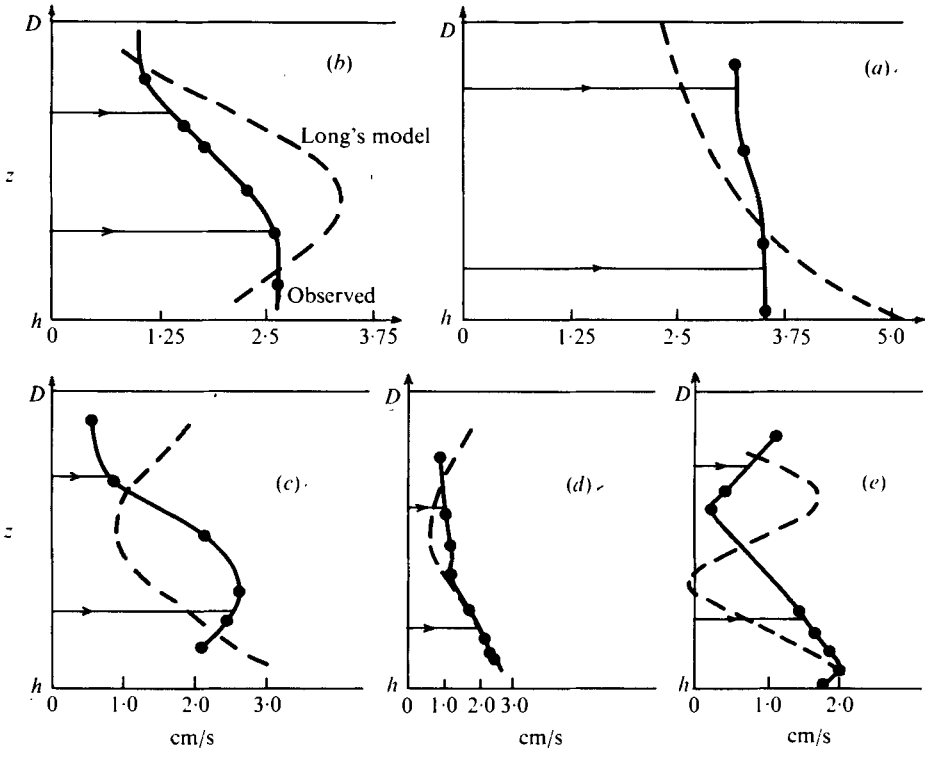

FIGURE 3. Velocity profiles over the crest of the obstacle for various values of K for steady-state conditions compared with the corresponding curves obtained from Long's model. $h/D = 0{\cdot}12$ for all cases. The points on the experimental curves denote the observations. (*a*) $K = 1{\cdot}21$; (*b*) $K = 1{\cdot}97$; (*c*) $K = 2{\cdot}23$; (*d*) $K = 2{\cdot}58$; (*e*) $K = 3{\cdot}83$.

As another check on Long's model, the velocity profiles directly above the top of the obstacle were compared for a number of cases under the same circumstances as above. The comparison between these is shown in figure 3 and the agreement is very poor. A close inspection of the comparative figures of Davis (1969) and Long (1955) reveals similar differences in many cases: although the patterns of the streamlines are generally similar, the spacings between them often are not.

Hence Long's model gives a poor description of detailed aspects of the flow field even for quite small smooth obstacles, although the general picture of the lee-wave field is roughly correct: it would be strange, in fact, if the latter were not so, since the wavelengths of the lee waves must be correctly obtained. The model may be more accurate if the obstacle height is smaller, but in this case it may be no improvement on the simpler linear perturbation theory.

4. Downstream observations

Stagnant regions or 'rotors' occur in the lee waves when their amplitude is sufficiently high. Figure 4 (plate 2) shows four 'steady-state' flow patterns for a larger obstacle than in figure 2, in order of increasing K, showing the evolving character of the stagnant regions. Such regions contain fluid which is nearly stationary relative to the obstacle. The regions are closed with stagnation points upstream and downstream,

although there is a small leakage at the downstream end, apparently due to viscous effects, which is balanced by fluid added from the upstream side. Usually there is little evidence of rotation within the region unless it is attached to a boundary where a small amount of rotation is provided by tangential stress: hence the term 'rotor' is deemed inappropriate here, except for regions attached to the lower boundary, where the tangential stress may be large.

The downstream lee-wave field itself was not examined in detail in this study. However, some observations were made at a point downstream of the initial position of the obstacle in order to investigate possible effects of the downstream end of the tank, and to look for negatively propagating disturbances. For the latter, the kind envisaged in particular were the columnar modes of McIntyre (1972), generated by nonlinear interactions in the lee-wave tails. Observations and measurements from photographs taken by a stationary camera for two cases, $K = 1{\cdot}81$ and $K = 2{\cdot}71$, suggested the presence of very weak unsteady motions (< 1 mm/s), which would be negligible in comparison with the upstream and lee-wave motions under study. No motions of the character predicted by McIntyre were observed, which was not surprising because the theoretical velocity magnitudes for these cases are less than 0·02 mm/s. The downstream end of the tank was thus seen to have a negligible effect on the flow, until the arrival of motions reflected from the upstream end.

5. Upstream observations

It seemed likely that the failure of Long's model, as described in § 3, was due to the breakdown of Long's hypothesis concerning upstream effects, and so a series of observations upstream of the obstacle was made. For these the camera was situated at a fixed position relative to the tank, 1·7 m or 1·9 m upstream from the starting position of the obstacle. Streak photographs were taken at regular time intervals. Since the fluid velocities were expected to be somewhat smaller than those observed in the lee waves, comparatively longer time exposures (of several seconds) were used. Figures 5 and 7 (plates 3–8) show several series of observations made using this procedure, in order of increasing K. The upstream end of the tank has no effect on the figures and motions described unless stated otherwise.

Series (*a*) in figure 5 (plate 3) shows a sequence of 4 s exposures taken at 10 s intervals (from start to start) with $K = 0{\cdot}91$ (for details see figure caption), so that no lee-wave modes were present. The figures visible near the bottom of the tank denote distance from the left-hand end of the tank in centimetres, and motion was always begun with the obstacle centred on 310 cm and the digital clock (top right, showing minutes and seconds) showing zero seconds. Exposures were begun at multiples of 10 s after the start (the right-hand digit always reads '8' owing to superposition of numerals). The obstacle appears blurred at the bottom in the third, fourth and fifth frames, and the fluid motion, which is in the forward direction (i.e. from right to left) in front of the obstacle at the bottom, has some similarity to potential flow. The modifications due to the density gradient (with presumably some incidental viscous effects) introduce an asymmetry into the streamline pattern, so that the region of rising motion in front of the obstacle is broadened and the region of descending motion behind it is shortened. There is also an indication that the descending motion is too strong, resulting in an

extended region of weak rising motion behind the obstacle, with a return flow of forward motion near the upper boundary. The flow pattern near the obstacle appeared to be steady. One interesting feature is that, after the obstacle was stopped near the left-hand end of the tank, the fluid motion continued, was reflected from the end wall and travelled back down the tank with the speed of an internal gravity wave appropriate to its length ($\sim 0{\cdot}7\ ND/\pi$).

Series (*b*) in figure 5 (plate 4) is identical with series (*a*) except that the obstacle speed has been decreased so that $K = 1{\cdot}20$. The flow is now subcritical with respect to the first internal-wave mode and the flow field is much more asymmetrical than before. The front of the upstream motion now has the character of a shear front (McEwan & Baines 1974), and is propagating ahead of the obstacle at the long-wave speed ND/π. The fluid which is consequently lifted up ahead of the obstacle descends over and behind it into the first lee-wave mode, which is evident in the final frame.

In series (*c*) in figure 5 (plate 5) K has been increased to 2·0 and the large obstacle has been used, but still with 4 s exposures. The motion is now more complicated, with oscillations in the amplitude of mode 1 upstream; mode 2, on the verge of propagating, is prominent close to the obstacle in the final frame. Series (*d*) (plate 6) shows the motion with U decreased so that $K = 2{\cdot}52$, other conditions remaining the same as in series (*c*); mode 2 has now propagated some distance ahead of the obstacle, the velocity at the lower boundary again being in the forward direction. Series (*e*) (plate 7) shows a different set of conditions with $K = 5{\cdot}9$, again with 4 s exposures. The theoretical positions of the upstream fronts $n = 1$–5 (based on the long-wave speeds $ND/n\pi$) are indicated by the arrows at the bottom, and these are seen to be consistent with the observed flow, although the picture is complicated by the reflexion of the first mode from the upstream end of the tank, which affects frames 5–8. The most prominent feature of the flow as K is increased is the partial blocking below the top of the obstacle, which is added to with each successive mode, together with a strong reversed flow upstream just above the level of the top of the obstacle (or as close to it as the modal structure will permit). On passing over the obstacle this 'jet' pours down the lee side. Other jet-like motion above this major jet is also related to the lee-wave structure (see figures 2 and 4).

The maximum horizontal velocities (relative to the tank) in upstream modes 1 and 2 are shown in figures 6(*a*) and (*b*) respectively. These are the velocities of the initial maxima, and subsequent velocities in the modes (i.e. before the obstacle arrives) may be variable and smaller. Nevertheless, these figures indicate that the upstream effects are of first order in the obstacle height h. It is interesting to compare these observations with results from the theory of Wong & Kao (1970) for a semi-infinite obstacle of the same height, modelled by a source. The latter are shown by the dashed curves in figures 6 (*a*) and (*b*) and are suggestive, but are not intended as a fit to the data.

The phenomena described above are essentially inviscid and hydraulic in character. It is possible to argue that all the upstream effects for (say) $1 < K < 3$ are transient and that the tank is too short to resolve this; however, this seems unlikely since it would be inconsistent with the observations for larger K and is also contradicted by the results of Wei *et al.* (1975) in a much longer tank. Hence the above observations indicate that the reason for the inapplicability of Long's model is the invalidity of the 'no upstream influence' hypothesis when $K > 1$. The manner in which this assumption manifests itself in Long's model may be seen from the following argument. If one

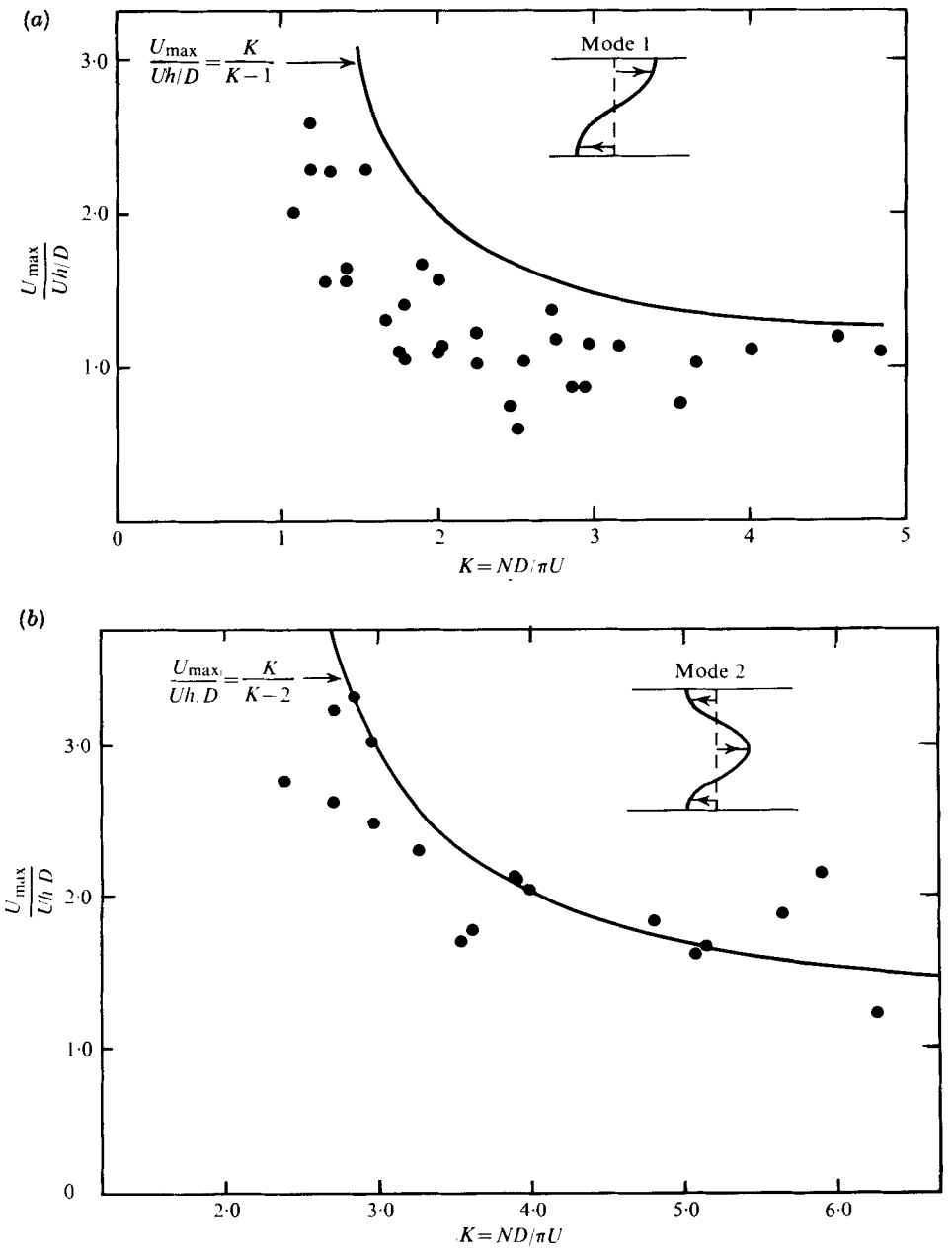

FIGURE 6. Maximum fluid velocities (measured near the top and bottom for the first mode and near the mid-depth for the second mode) in the initial maximum of upstream motion, scaled with Uh/D, as a function of K for (*a*) mode 1 and (*b*) mode 2. The solid curves are from the theory of Wong & Kao (1970) for a semi-infinite obstacle modelled by a source, and are presented for comparison only.

examines the behaviour of the Green's function G for Long's model [equation (3.4)] for K near unity (for example), one notices that, for $K < 1$, G contains a term

$$\pi^{-1}\alpha_1^{-1} \exp(-\alpha_1 |x-\xi|) \sin\eta \sin z,$$

where $\alpha_1 = |K^2-1|^{\frac{1}{2}}$, which is exponentially decaying in x both upstream and downstream with exponent α_1. As $K \to 1-$, $\alpha_1 \to 0$, so that the horizontal exponential decay is very small. As K becomes greater than unity, the corresponding term in Long's model becomes oscillatory in $x-\xi$ on the downstream side, with wavenumber α_1, but it is identically zero on the upstream side, as a consequence of Long's hypothesis. However, it is evident from figures 5 (*a*) and (*b*) that this is not the case in practice at all, the decaying motion upstream converting to a wavelike motion which (ideally) propagates to infinity. A similar phenomenon occurs for the higher modes ($n = 2, 3, \ldots$) when K is increased beyond 2, 3, ... Hence the 'no upstream influence' assumption is seen to be an arbitrary one of mathematical convenience, and it is not surprising that the magnitude of the error obtained is sufficient to account for the discrepancies reported in § 3.

The situation when K becomes large is shown in figure 7 (*a*) (plate 8), where $K = 11{\cdot}3$, with a 4 s exposure. In this case some of the eleven upstream modes will have propagated up and down the length of the tank several times, so that end effects are important. The fluid below the level of the top of the obstacle is almost completely blocked, rising in a region near the end of the tank to the level of the upstream jet, in which it pours over the obstacle and down the lee side. Above this level the velocities are smaller and more variable. The motion on the downstream side, apart from the lee waves, had the appearance of being the mirror image of that on the upstream side, with motion away from the obstacle at the lowest level leading to rising motion downstream and return flow at the level of the upstream jet. This general behaviour persisted as U was decreased further so that K increased to approximately 40. In the limit of very slow flow, viscous and diffusive effects will become important (e.g. Barnard & Pritchard 1975) but these are not under discussion here. If the depth is decreased so that

$$h < D \lesssim 2h,$$

the motion is dominated by the first mode, as shown in figure 7 (*b*) (plate 8), where $K = 4{\cdot}9$. The character of the flow is in many ways similar to that in figure 7 (*a*), the downstream motion appearing to be the 'mirror image' of the upstream motion, with the lee waves superimposed.

6. Conclusions

It has been shown that Long's model provides a poor description of detailed aspects of the flow field in fluid of finite depth in the areas in which it is expected to be most useful, viz. criteria for the onset of instability in the lee waves and associated velocity profiles over the top of the obstacle. The reason for this is apparently the breakdown of Long's hypothesis, since the motion of the obstacle generates a series of shear fronts (or columnar disturbance modes) upstream corresponding to the lee waves downstream, with magnitudes which are proportional to the obstacle height. This upstream motion has a complex structure which is described qualitatively in § 5; the most important feature is that, as U decreases, the fluid below the top of the obstacle becomes partially blocked. This results in rising motion (associated with the shear fronts), and the

elevated fluid forms a horizontal jet which then pours over and down the lee side of the obstacle.

The empirical curve for the onset of gravitational instability in the lee waves is given in figure 1, and may be roughly approximated by

$$H = \pi h/D = 0{\cdot}28 + 0{\cdot}37/K,$$

or

$$R = Nh/U = 0{\cdot}28\,K + 0{\cdot}37, \quad 1 < K < 4, \tag{6.1}$$

for the Witch of Agnesi profile with $a/D \simeq 0{\cdot}2$, where the uncertainty in both figures is approximately $\pm\, 0{\cdot}05$.

The question than arises as to what Long's model actually means. It is still expected to give the correct solution (i.e. the flow field obtained at large times after starting the obstacle from rest) when $K < 1$. For $K > 1$ (but not an integer) it will give the flow field when the upstream wave motion generated for an initially non-uniform *unknown* $\rho(z)\,U(z)^2$ profile *exactly cancels out* the initial variations in $\rho(z)\,U(z)^2$ far upstream.

It should be noted that the conclusions given here apply specifically to fluid of finite depth. The situation for infinite depth, and the reasons why the analysis of McIntyre (1972) did not predict the observed upstream effects, will be discussed in a future paper (Baines 1977).

The author is grateful to Dr Angus McEwan, who participated in the early stages of the experimental side of this investigation, to Ross Hall and George Scott for assistance with the experiments, and to the National Environmental Research Council of Great Britain for a Fellowship at the Department of Applied Mathematics and Theoretical Physics, Cambridge, where this work was written up.

REFERENCES

Baines, P. G. 1977 Inviscid stratified flow over finite two-dimensional obstacles in fluid of infinite depth. In preparation.

Barnard, B. J. S. & Pritchard, W. G. 1975 The motion generated by a body moving through a stratified fluid at large Richardson numbers. *J. Fluid Mech.* **71**, 43.

Benjamin, T. B. 1970 Upstream influence. *J. Fluid Mech.* **40**, 49.

Davis, R. E. 1969 The two-dimensional flow of a stratified fluid over an obstacle. *J. Fluid Mech.* **36**, 127.

Drazin, P. G. & Moore, D. W. 1967 Steady two-dimensional flow of a fluid of variable density over an obstacle. *J. Fluid Mech.* **28**, 353.

Droughton, J. V. & Chen, C. F. 1971 Channel flow of a density stratified fluid about immersed bodies. *J. Basic Engng* **94**, 122.

Grimshaw, R. 1968 A note on the steady two-dimensional flow of a stratified fluid over an obstacle. *J. Fluid Mech.* **33**, 293.

Huppert, H. E. & Miles, J. W. 1969 Lee waves in a stratified flow. Part 3. Semi-elliptical obstacle. *J. Fluid Mech.* **55**, 481.

Long, R. R. 1955 Some aspects of the flow of stratified fluids. III. Continuous density gradients. *Tellus* **7**, 343.

McEwan, A. D. & Baines, P. G. 1974 Shear fronts and an experimental stratified shear flow. *J. Fluid Mech.* **63**, 257.

McIntyre, M. E. 1972 On Long's hypothesis of no upstream influence in uniformly stratified or rotating flow. *J. Fluid Mech.* **52**, 209.

Maxworthy, T. 1970 The flow created by a sphere moving along the axis of a rotating slightly viscous fluid. *J. Fluid Mech.* **40**, 453.

MILES, J. W. 1968*a* Lee waves in a stratified flow. Part 1. Thin barrier. *J. Fluid Mech.* **32**, 549.

MILES, J. W. 1968*b* Lee waves in a stratified flow. Part 2. Semi-circular obstacle. *J. Fluid Mech.* **33**, 803.

MILES, J. W. 1972 Axisymmetric rotating flow past a circular disk. *J. Fluid Mech.* **53**, 689.

MILES, J. W. 1975 Axisymmetric rotating flow past a prolate spheroid. *J. Fluid Mech.* **72**, 363.

MILES, J. W. & HUPPERT, H. E. 1969 Lee waves in a stratified flow. Part 4. Perturbation approximations. *J. Fluid Mech.* **35**, 497.

PAO, Y.-H. 1969 Inviscid flows of stably stratified fluids over barriers. *Quart. J. Roy. Met. Soc.* **95**, 104.

PEKELIS, Y. M. 1972 Solution of the problem of flow past an obstacle. *USSR Gidromet. Nauch-Issl. Trentr. SSSR, Leningrad, Trudy* **99**, 63.

PRITCHARD, W. G. 1969 The motion generated by a body moving along the axis of a uniformly rotating fluid. *J. Fluid Mech.* **39**, 443.

SEGUR, H. 1971 A limitation on Long's model in stratified flows. *J. Fluid Mech.* **48**, 161.

TRUSTRUM, K. 1964 Rotating and stratified fluid flow. *J. Fluid Mech.* **19**, 415.

TURNER, J. S. 1973 *Buoyancy Effects in Fluids.* Cambridge University Press.

WEI, S. N., KAO, T. W. & PAO, H.-P. 1975 Experimental study of upstream influence in the two-dimensional flow of a stratified fluid over an obstacle. *Geophys. Fluid Dyn.* **6**, 315.

WONG, K. K. & KAO, T. W. 1970 Stratified flow over extended obstacles and its application to topographical effect on ambient wind shear. *J. Atmos. Sci.* **27**, 884.

YIH, C.-S. 1960 Exact solutions for steady two-dimensional flow of a stratified fluid. *J. Fluid Mech.* **9**, 161.

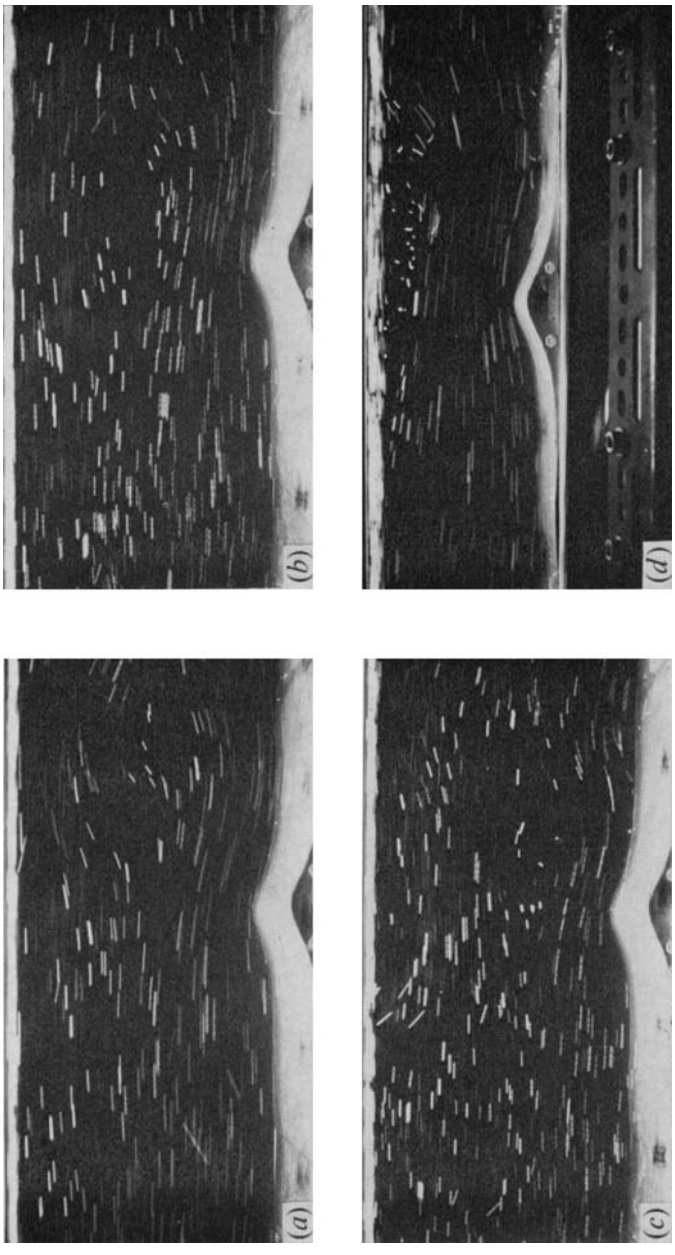

FIGURE 2. Some examples of steady-state lee-wave fields corresponding to points in figure 1. (*a*) $H = \pi h/D = 0{\cdot}36$, $K = 2{\cdot}39$ (stable), $U = 1{\cdot}83$ cm/s; (*b*) $H = 0{\cdot}36$, $K = 2{\cdot}83$ (stable), $U = 1{\cdot}55$ cm/s; (*c*) $H = 0{\cdot}36$, $K = 3{\cdot}98$ (marginally unstable), $U = 1{\cdot}10$ cm/s; (*d*) $H = 0{\cdot}60$, $K = 1{\cdot}56$ (unstable), $U = 1{\cdot}54$ cm/s. The camera is stationary relative to the obstacle.

(*Facing p.* 160)

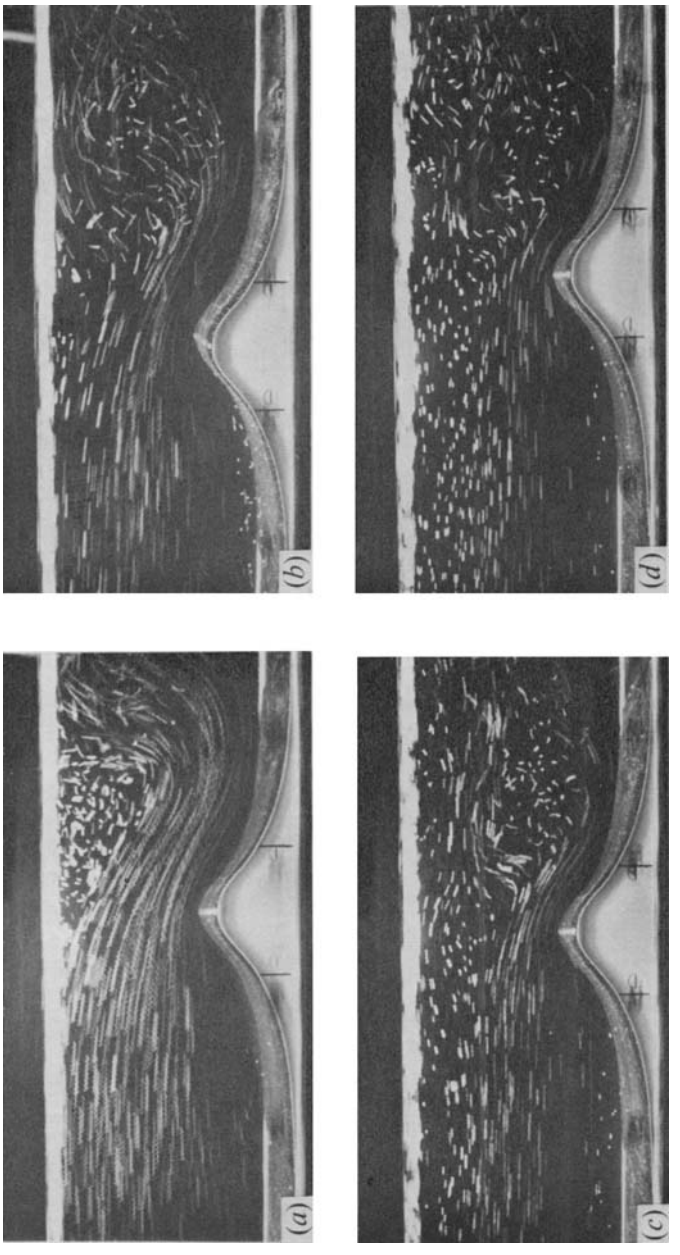

FIGURE 4. Some examples of stagnant regions embedded in lee-wave fields. All exposure times are 0·6 s, with $H = 1{\cdot}02$. (*a*) $K = 1{\cdot}82$, $U = 3{\cdot}85$ cm/s; (*b*) $K = 2{\cdot}1$, $U = 3{\cdot}3$ cm/s; (*c*) $K = 3{\cdot}3$, $U = 2{\cdot}1$ cm/s; (*d*) $K = 4{\cdot}1$, $U = 1{\cdot}7$ cm/s. (Small-scale oscillations in the streaks for (*a*) and (*b*) are probably due to carriage vibration.) The camera is stationary relative to the obstacle.

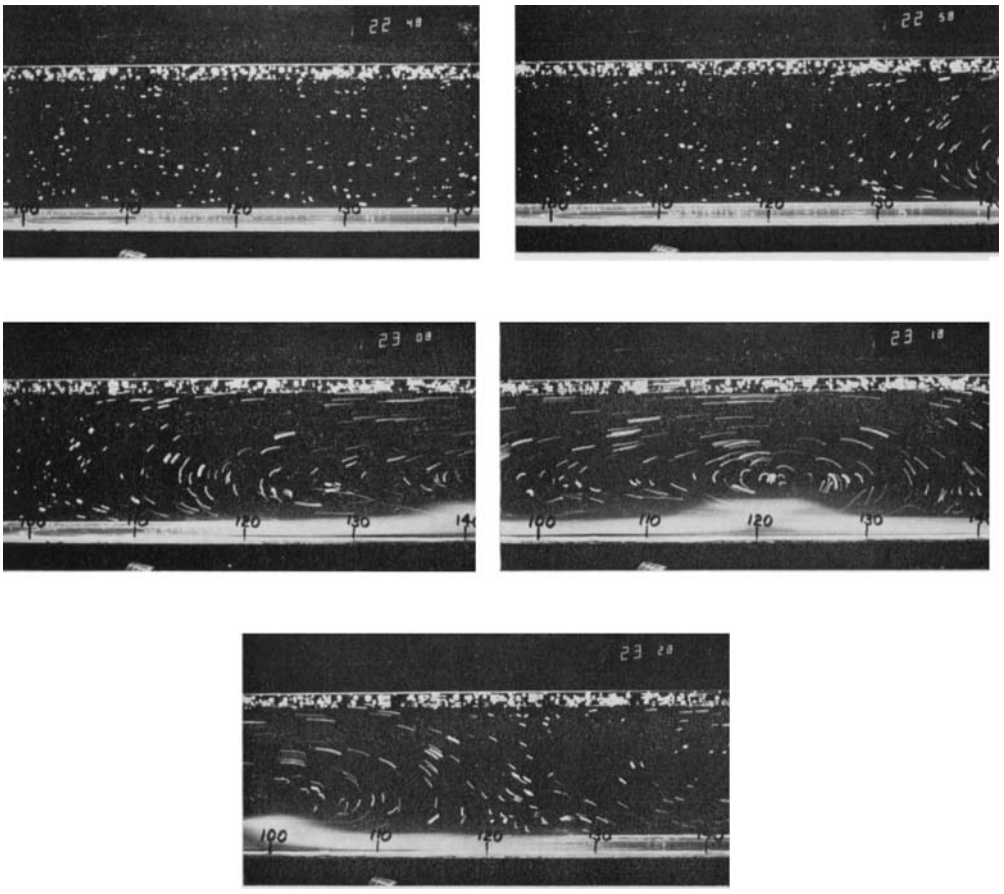

(*a*)

FIGURE 5. Series of streak photographs taken by a stationary camera upstream of the obstacle. The time exposures are all of 4 s duration, beginning 10 s apart unless otherwise stated. (*a*) $H = 0{\cdot}36$, $K = 0{\cdot}91$, $U = 2{\cdot}64$ cm/s; (*b*) $H = 0{\cdot}36$, $K = 1{\cdot}2$, $U = 2{\cdot}01$ cm/s; (*c*) $H = 1{\cdot}02$, $K = 2{\cdot}0$, $U = 3{\cdot}09$ cm/s; (*d*) $H = 1{\cdot}03$, $K = 2{\cdot}52$, $U = 2{\cdot}27$ cm/s; (*e*) $H = 0{\cdot}64$, $K = 5{\cdot}9$, $U = 1{\cdot}53$ cm/s. (In (*c*) and (*d*) the upstream velocity profiles are not quite sinusoidal, because the density gradient near the bottom has been weakened by mixing due to previous runs.) In (*e*) the arrows denote theoretical positions of the fronts of the corresponding modes.

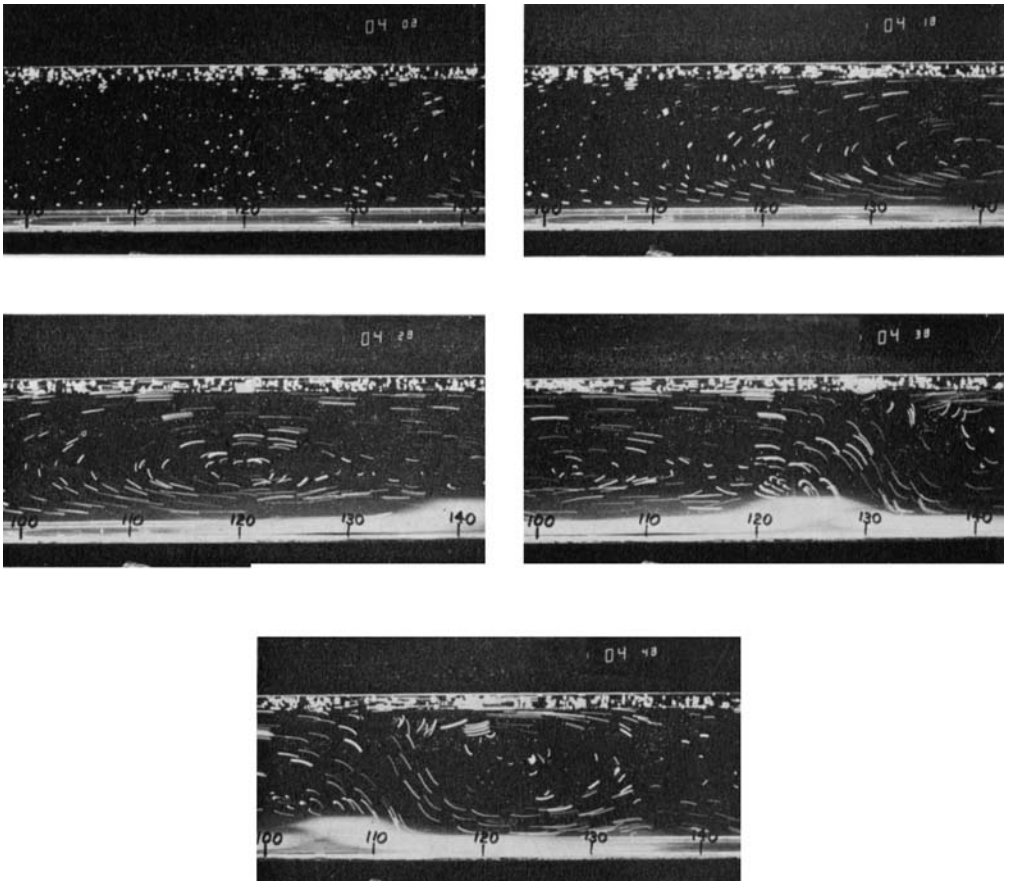

FIGURE 5 (*b*). For legend see plate 3.

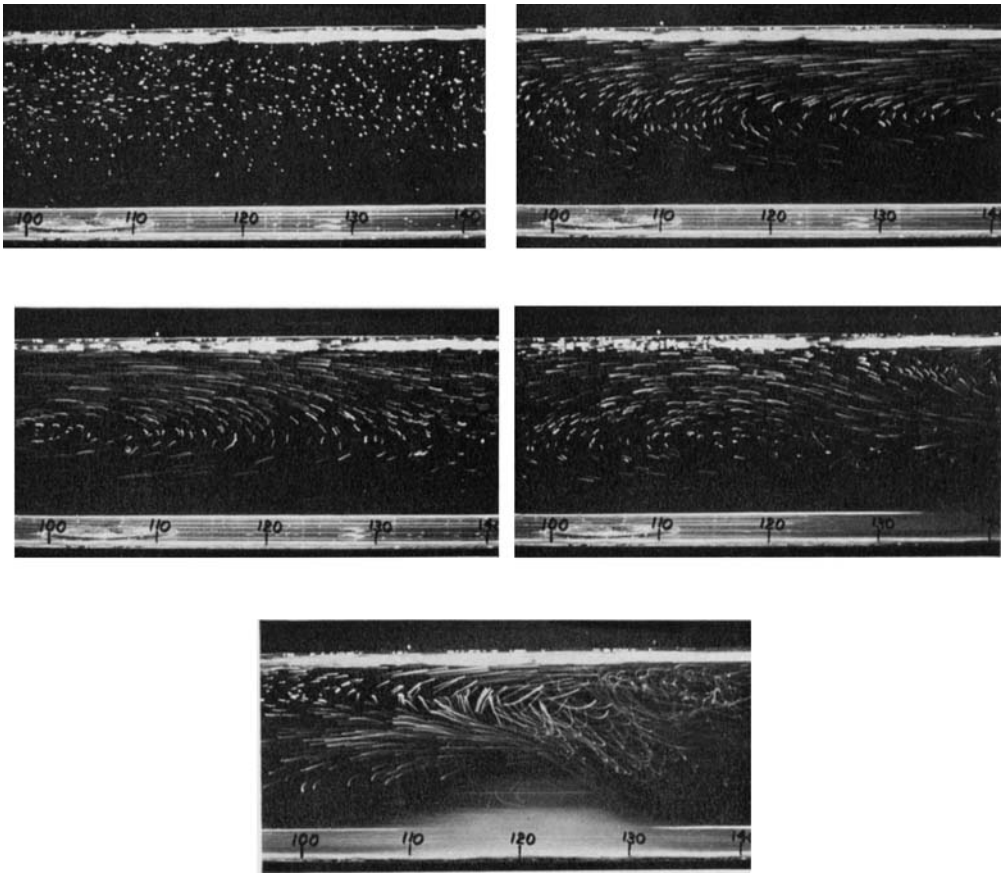

FIGURE 5(*c*). For legend see plate 3.

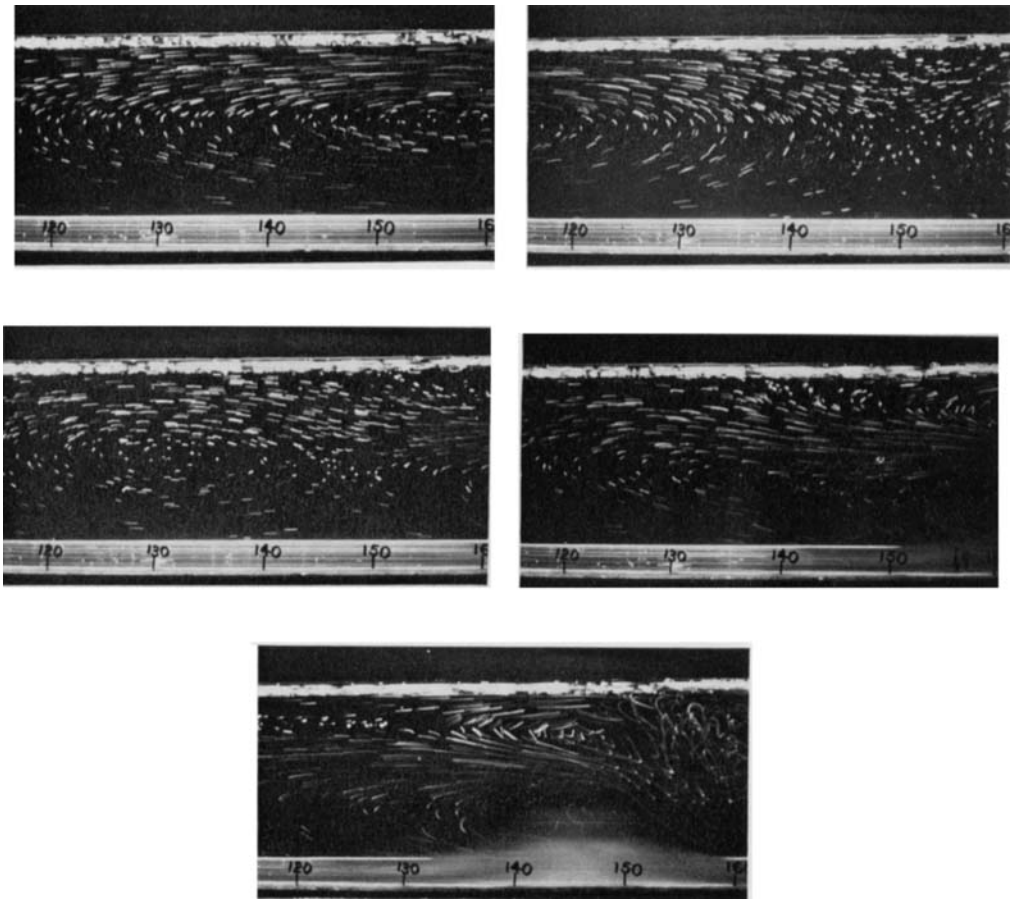

FIGURE 5(*d*). For legend see plate 3.

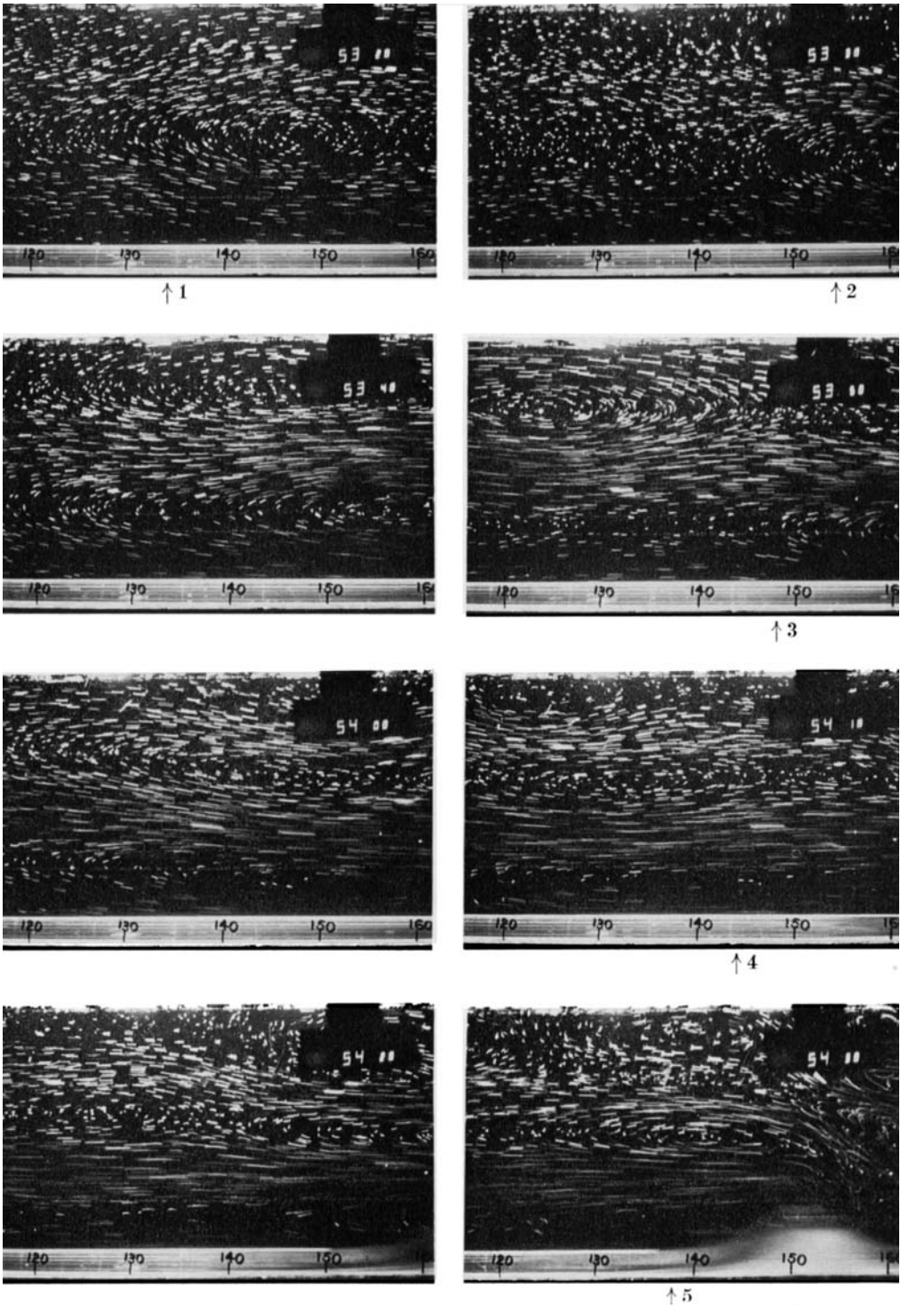

FIGURE 5(*e*). For legend see plate 3.

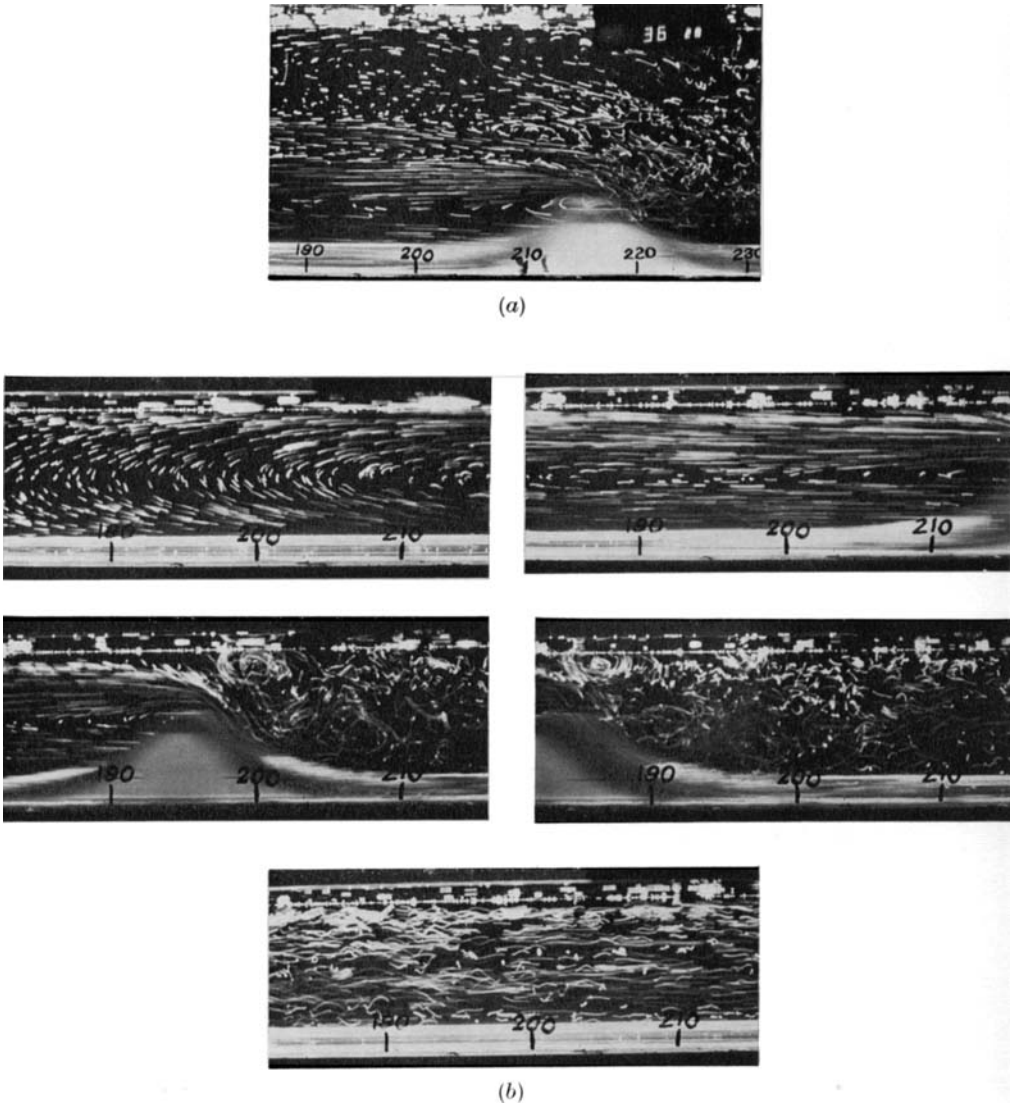

(*a*)

(*b*)

FIGURE 7. As for figure 5, but for (*a*) large K and (*b*) shallow depth. (*a*) $H = 0{\cdot}79$, $K = 11{\cdot}3$, $U = 0{\cdot}66$ cm/s; (*b*) $H = 1{\cdot}67$, $K = 4{\cdot}94$, $U = 0{\cdot}67$ cm/s, with 8 s exposures beginning 20, 80, 110, 130 and 150 s after the start.